



**HAL**  
open science

## Non-collinear ordering of the orbital magnetic moments in magnetite

H Elnaggar, Ph Saintavit, A. Juhin, S. Lafuerza, F. Wilhelm, A. Rogalev,  
M.-A Arrio, Christian Brouder, M van Der Linden, Z. Kakol, et al.

► **To cite this version:**

H Elnaggar, Ph Saintavit, A. Juhin, S. Lafuerza, F. Wilhelm, et al.. Non-collinear ordering of the orbital magnetic moments in magnetite. *Physical Review Letters*, 2019, 123, 10.1103/PhysRevLett.123.207201 . hal-02349259

**HAL Id: hal-02349259**

**<https://hal.science/hal-02349259v1>**

Submitted on 5 Nov 2019

**HAL** is a multi-disciplinary open access archive for the deposit and dissemination of scientific research documents, whether they are published or not. The documents may come from teaching and research institutions in France or abroad, or from public or private research centers.

L'archive ouverte pluridisciplinaire **HAL**, est destinée au dépôt et à la diffusion de documents scientifiques de niveau recherche, publiés ou non, émanant des établissements d'enseignement et de recherche français ou étrangers, des laboratoires publics ou privés.

# Non-collinear ordering of the orbital magnetic moments in magnetite

H. Elnaggar,<sup>1,\*</sup> Ph. Sainctavit,<sup>2</sup> A. Juhin,<sup>2</sup> S. Lafuerza,<sup>3</sup> F. Wilhelm,<sup>3</sup> A. Rogalev,<sup>3</sup> M.- A. Arrio,<sup>2</sup> Ch. Brouder,<sup>2</sup> M. van der Linden,<sup>1</sup> Z. Kakol,<sup>4</sup> M. Sikora,<sup>5</sup> M. W. Haverkort,<sup>6</sup> P. Glatzel,<sup>3</sup> and F. M. F. de Groot<sup>1,†</sup>

<sup>1</sup>*Debye Institute for Nanomaterials Science, Utrecht University, 3584 CA Utrecht, The Netherlands.*

<sup>2</sup>*Institute de Mineralogie de Physique des Matériaux et de Cosmochimie, Sorbonne Université, CNRS, 4 place Jussieu, Paris, France.*

<sup>3</sup>*European Synchrotron Radiation Facility, CS40220, F-38043 Grenoble Cedex 9, France.*

<sup>4</sup>*Faculty of Physics and Applied Computer Science,*

*AGH University of Science and Technology, Mickiewicza 30, 30-059 Krakow, Poland.*

<sup>5</sup>*Academic Centre for Materials and Nanotechnology,*

*AGH University of Science and Technology, Mickiewicza 30, 30-059 Krakow, Poland.*

<sup>6</sup>*Institut für Theoretische Physik, Universität Heidelberg, Philosophenweg 19, 69120 Heidelberg, Germany.*

(Dated: July 16, 2019)

The magnitude of the orbital magnetic moment [1–9] and its role as a trigger of the Verwey transition [10–17] in the prototypical Mott insulator, magnetite, remain contentious. Using  $1s2p$  resonant inelastic X-ray scattering magnetic linear angular distribution (RIXS-MLAD), we prove the existence of non-collinear orbital magnetic ordering and infer the presence of dynamical distortion creating a polaronic precursor for the metal to insulator transition. These conclusions are based on a subtle angular shift of the RIXS-MLAD spectral intensity as a function of the magnetic field orientation. Theoretical simulations show that these results are only consistent with non-collinear magnetic orbital ordering. To further support these claims we perform Fe  $K$ -edge X-ray magnetic circular dichroism (XMCD) in order to quantify the iron average orbital magnetic moment.

Magnetite ( $[\text{Fe}^{3+}]_A[\text{Fe}^{3+}, \text{Fe}^{2+}]_B\text{O}_4$ ) is the most abundant iron bearing mineral on Earth and it finds many applications in areas such as palaeomagnetism, medicine, data recording, and engineering [18]. Ever since Verwey’s pioneering work [19], an immense amount of research has been dedicated to  $\text{Fe}_3\text{O}_4$  in view of its importance as a reference for systems exhibiting the metal to insulator transition [11, 20, 21]. In  $\text{Fe}_3\text{O}_4$ , the Verwey transition occurs at  $T_V \sim 125$  K and results in a spontaneous change of both, the lattice symmetry and the electric conductivity. Above  $T_V$   $\text{Fe}_3\text{O}_4$  has a cubic inverse spinel crystal structure containing two different Fe sites.  $\text{Fe}^{3+}$  ions reside in tetrahedral ( $T_d$ ) interstices (the A sites) while both  $\text{Fe}^{2+}$  and  $\text{Fe}^{3+}$  ions reside in octahedral ( $O_h$ ) interstices (the B sites). The A and B sublattices are antiferromagnetically coupled while the Fe ions in the same sublattice are ferromagnetically coupled (Fig. 1a).

In ferromagnets and ferrimagnets, the spin and orbital magnetic moments of the transition metal ions can be directly quantified by applying the sum rules on the  $L_{2,3}$  XMCD signal [22]. In spite of the great success of sum rules, the experimental and analysis procedures were shown to be prone to huge uncertainties due to surface effects [1]. Orbital magnetic moments as small as  $0.01 \mu_B$  [2] and as large as  $0.33 \mu_B$  [3] were reported for  $\text{Fe}_3\text{O}_4$ . In addition, large orbital magnetic moment contributions that are of equal absolute values but with antiparallel coupling between the Fe A and B sublattices were also suggested [4] (for a unit formula of  $\text{Fe}_3\text{O}_4$ :  $F_{eB} \mu_L = 1 \mu_B$  and  $F_{eA} \mu_L = -1 \mu_B$ ). A summary of the orbital and spin magnetic moments reported in literature using various techniques is shown in Fig. S1. These large discrepancies regarding an essential quantity to many Mott

insulators [23] ask for a new approach.

In this work we employed a combination of Fe  $K$ -edge XMCD and  $1s2p$  RIXS-MLAD measurements to investigate the orbital magnetic moment of Fe in  $\text{Fe}_3\text{O}_4$ . Experiments at the Fe  $K$ -edge ( $1s \rightarrow 3d + 4p$  excitations) have a probing depth of few  $\mu m$  and hence surface effects are negligible offering a valuable advantage over  $L_{2,3}$ -edge measurements. We quantified the average orbital magnetic moment by performing  $K$ -edge XMCD. The accurately measured  $1s2p$  RIXS-MLAD signal was used to determine the average square orbital magnetic moment which complements the average quantity obtained from XMCD. A difference between the orbital magnetic moment predicted by both experiments indicates compensation: the orbital magnetic moments of the Fe ions must be either antiparallel or non-collinear.

Guided by theoretical calculations, we show that the only possibility to explain both of our experimental results is the existence of a non-collinear magnetic orbital ordering that can tilt the orbital magnetic moment as large as  $82^\circ$  away from the spin magnetic moment. We proposed a model for this non-collinear orbital magnetic ordering and inferred the presence of a dynamical distortion related to the  $X_3$  phonon mode in the high temperature phase. Our model imposes strong restrictions on the candidate mechanisms for the Verwey transition [10, 24].

We investigated highly stoichiometric (001), (110) and (111)  $\text{Fe}_3\text{O}_4$  single crystals at room temperature. The average orbital magnetic moment projected along the magnetic field direction can be quantified by performing Fe  $K$  pre-edge XMCD measurements [22]. Three main dichroic features can be seen at  $E_I = 7112.7$  eV,  $E_{II} = 7114$  eV and  $E_{III} = 7115.1$  eV with only significant angular de-

80 pence at the first feature (Fig. 1b). The co-existence  
 81 of two Fe sites in  $\text{Fe}_3\text{O}_4$  complicates the direct analysis  
 82 of the XMCD signal and renders a full calculation impor-  
 83 tant to assign spectral features to the specific Fe species.

84 Configuration interaction calculations taking into ac-  
 85 count *i*)- intra-atomic Coulomb interaction, *ii*)- crystal  
 86 field, *iii*)- spin-orbit coupling, and *iv*)- exchange inter-  
 87 action were performed using the quantum many-body  
 88 program Quany [25–27]. Our theoretical simulations  
 89 show that the feature at  $E_I$  arises mainly from electric  
 90 quadrupole transitions (*i.e.*  $1s \rightarrow 3d$  excitations) at the  
 91 formal  $\text{Fe}^{2+}$  ions while the features at  $E_{II}$  and  $E_{III}$  arise  
 92 mainly from electric dipole transitions (*i.e.*  $1s \rightarrow 3d+4p$   
 93 excitations) at the  $\text{Fe}^{3+} T_d$  ions due to onsite  $3d-4p$   
 94 orbital mixing as discussed by Westre *et. al.* [28]. The  
 95 quadrupolar signals from the  $\text{Fe}^{3+}$  A and B sites nearly  
 96 cancel out as shown in Fig. S8.

97 The experimental XMCD signal and its angular de-  
 98 pendence can be best interpreted to arise from a par-  
 99 tially quenched orbital magnetic moment at the formal  
 100  $\text{Fe}^{2+}$  ions. An excellent agreement between the calcu-  
 101 lation and the experiment is observed (compare spectra  
 102 labelled Exp and Calc 1 in Fig. 1b). This partial quench-  
 103 ing is a result of the octahedral symmetry accompanied  
 104 by a small trigonal distortion ( $D_\sigma = 67 \pm 10$  meV). The  
 105 Fe environment is not perfectly  $O_h$  since the point group  
 106 symmetry of the B site is rhombohedral ( $D_{3d} \equiv \bar{3}m$ ).  
 107 We found that the average orbital magnetic moment is  
 108  $0.26 \pm 0.03 \mu_B$  per unit formula of  $\text{Fe}_3\text{O}_4$ . It is impor-  
 109 tant to note that feature I is theoretically predicted to  
 110 be completely suppressed in the case that  $\mu_L = 0 \mu_B$  (see  
 111 Fig. 1b Calc 2) strongly supporting the presence of a  
 112 finite orbital magnetic moment in bulk  $\text{Fe}_3\text{O}_4$ .

113 To investigate possible non-collinearity of the orbital  
 114 magnetic moment, we performed comprehensive  $1s2p$   
 115 RIXS-MLAD measurements. This complements the av-  
 116 erage projected result obtained from XMCD. The RIXS-  
 117 MLAD was measured by rotating the sample about the  
 118 incident wave-vector direction ( $\mathbf{k}_{in}$ ) aligned with the  
 119  $[110]$  direction (refer to Fig. 2a). This implies that the  
 120 RIXS-MLAD includes contributions from both structural  
 121 and magnetic dichroism signals. We focus in this work on  
 122 the effect of the magnetic dichroism on the linear angular  
 123 distribution of RIXS. We initially measured the RIXS-  
 124 MLAD with the magnetic field *nearly* parallel to  $\mathbf{k}_{in}$  as  
 125 a reference measurement. In this case the magnetic field  
 126 is oriented along a high symmetry crystallographic direc-  
 127 tion and the angle between the linear incident polariza-  
 128 tion ( $\epsilon_{in}$ ) and the magnetic field *nearly* does not change  
 129 as a function of the sample rotation. These choices sim-  
 130 plify the angular dependence and serve as a benchmark  
 131 to analyze the RIXS spectra.

132 Although the experimental RIXS planes measured in  
 133 the horizontal ( $\phi = 0^\circ$ ) and vertical ( $\phi = 90^\circ$ ) config-  
 134 urations show a broad single pre-edge peak (Fig. S9a  
 135 and b), it is possible to identify three main features in

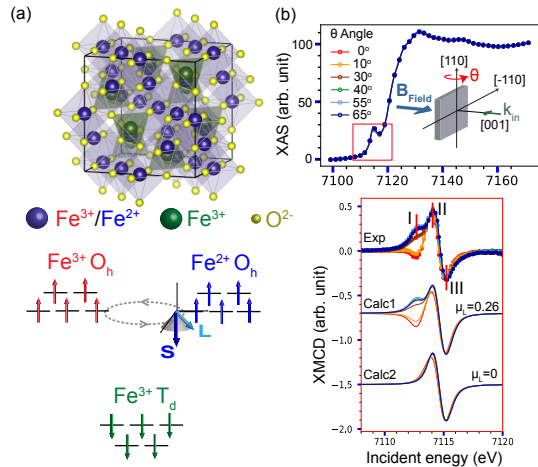


FIG. 1. (a) The unit cell of  $\text{Fe}_3\text{O}_4$  and the magnetic coupling between the Fe sites. Octahedral ( $O_h$ )  $\text{Fe}^{3+}$  and  $\text{Fe}^{2+}$  ions are antiferromagnetically coupled to the tetrahedral ( $T_d$ )  $\text{Fe}^{3+}$  ions. (b) Fe  $K$ -edge measurements in  $\text{Fe}_3\text{O}_4$  single crystal. The top panel shows XAS results as a function of the sample azimuthal angle  $\theta$ . The bottom panel shows the corresponding XMCD experimental (dotted) and theoretical (solid) Fe pre-edge signal. Two model calculations are presented: *i*)- Calc 1 is the optimized calculation where a partially quenched orbital magnetic moment of  $0.26 \mu_B$  per unit formula of  $\text{Fe}_3\text{O}_4$  was concluded, and *ii*)- Calc 2 is the theoretically expected XMCD signal for a fully quenched orbital magnetic moment scenario.

136 the experimental dichroism signal (Fig. 2b). Theoretical  
 137 calculation of the RIXS dichroism signal shows that the  
 138 quadrupolar contributions of the  $\text{Fe}^{3+} T_d$  and  $O_h$  sites  
 139 nearly cancel out (see Fig. S10) and hence the three fea-  
 140 tures labelled in Fig. 2b are dominantly attributed to the  
 141 formal  $\text{Fe}^{2+}$  ions. This is consistent with the XMCD re-  
 142 sults, where we found that the angular dependence is only  
 143 visible at the  $\text{Fe}^{2+}$  ions. The calculated RIXS dichroic  
 144 plane of the formal  $\text{Fe}^{2+}$  ions reproduces the three main  
 145 spectral features. The calculation only misses a weak fea-  
 146 ture at incident energy  $\sim 7115.1$  eV which is associated  
 147 with the electric dipole transition at the  $\text{Fe}^{3+}$  A site due  
 148 to onsite  $3d-4p$  orbital mixing.

149 The full  $360^\circ$  experimental (theoretical) angular de-  
 150 pendence of the three main spectral features can be seen  
 151 in Fig. 2c. The angular dependence is twofold and a  
 152  $90^\circ$  angular shift is observed between the first feature  
 153 and both the second and third features. A first expla-  
 154 nation of the general angular dependence can be pro-  
 155 vided by analysing the  $1s^1 3d^7$  intermediate states. Pro-  
 156 jections of the intermediate states associated with non-  
 157 zero transition matrix elements onto cubic crystal field  
 158 (*i.e.*  $O_h$ ) configurations were calculated using the pro-  
 159 gram CTM4DOC [29]. The first feature arises domi-  
 160 nantly from excitations to the  $t_{2g}$  orbitals, that are  $90^\circ$   
 161 angular shifted *w.r.t.* the second and third features cor-  
 162 responding to excitations dominantly into the  $e_g$  orbitals

[28]. We note that the angular dependence is anisotropic where the intensity of the third feature at  $\phi = 180^\circ$  is smaller than that at  $\phi = 0^\circ$ . This is related to the anisotropy in the detection in combination to a small misalignment angle ( $\delta$ ) of the magnetic field relative to the rotation axis *i.e.* the detector position relative to the sample as discussed in details in the Supplementary. In addition, our theoretical model assumes that the detection system is a single point while in reality four Ge (440) analyzer crystals were used. The minor discrepancy between the experiment and the calculations could be attributed to this fact.

We examined the coupling of the spin and orbital degrees of freedom by displacing the magnetic field  $50^\circ$  from the high symmetry [001] direction (refer to Fig. 3a). The orientation of the magnetic field corresponds to the  $[-\frac{\cos(40^\circ)}{\sqrt{2}}, \frac{\cos(40^\circ)}{\sqrt{2}}, \sin(40^\circ)]$  direction. Orienting the magnetic field in a low symmetry direction aligns the net spin magnetic moment parallel to the field. If the orbital magnetic moment is not fully quenched, it consequently re-aligns towards the low symmetry direction. The final orientation of the net magnetic moment depends on the strength of the competing interactions such as magnetic exchange, spin-orbit coupling and distortion. Hence, the angular shift of the maximum intensity of the excitations can be used to quantify magnetic-moment-induced distortion of the electron cloud. Based on this concept, we investigated the orbital magnetic moment of the formal  $\text{Fe}^{2+}$  ions. A careful analysis of the full  $360^\circ$  angular dependence exhibits a peculiar  $10^\circ$  angular shift of the maximum intensity between the second and third features in Fig. 3b.

Theoretical calculation of the angular dependences are presented in Fig. 3c. The model captures the essential aspects of the angular dependence and in particular the  $10^\circ$  angular shift of the maximum intensity. The angular shift ( $\Omega$ ) quantified by fitting the angular dependence to a  $\cos^2(\phi + \Omega)$  of the three features is reported in Tab. S4. The anisotropy of the angular dependence is not well reproduced, likely due to a small misalignment of the magnetic field that has not been included in the calculations (see Supplementary). It is now important to highlight the key ingredients responsible for this angular shift. The first factor is the static trigonal distortion. The relative orientation of the exchange interaction with respect to the local trigonal distortion varies between the four sites leading to anisotropic effects and generates four non-equivalent Fe B sites. The theoretical RIXS-MLAD for the four sites are shown in Fig. S12. The second factor is the effect of dynamical distortion that produces two subclasses of the Fe B sites, namely, sites 1 and 2 forming one subclass and sites 3 and 4 forming the other (see Fig. 4b). It is only when the dynamical distortion effect is taken into consideration that the experimental RIXS-MLAD angular shift can be reproduced (see Fig. S13).

An energy shift of  $\sim 0.2$  eV was found between the two subclasses.

We interpret the formation of these two subclasses as a result of a dynamical Jahn-Teller distortion at the Fe B sites. The magnitude of the static trigonal distortion lies close within the phonon energies of  $\text{Fe}_3\text{O}_4$  [30, 31], the magnetic exchange interaction and spin-orbit coupling, leading to a situation where electron-phonon interaction, dynamical Jahn-Teller and Kugel-Khomskii interactions all play a role in determining the low energy state. We treat this dynamical variation of the distortion in a first approximation as a small change in the bond lengths over the four sites giving rise to a small energy shift. This is a reasonable approximation because the electronic structure adapts almost instantaneously to the crystallographic structure (*i.e.* the electronic motion is much faster than the nuclear motion). In this case, the effect of phonons could be simulated as a static distribution of bond lengths leading to a shift in energy between the four sites. This is a common practice in XAS theory as can be found in the paper by Nemeusat *et al.* [32] where thermal fluctuations are simulated by a well chosen series of configurations. Although theoretical studies that treat simultaneously the electronic and the lattice degrees of freedom are required to comprehend the precise effect of the dynamical distortion, we point out that numerous theoretical works concluded the essential role of the strong electron-phonon coupling in the presence of strong electron correlations leading to dynamical Jahn-Teller distortion and the creation of polarons [33–36]. In particular, Piekarczyk *et al.* [33, 34] identified the highly dispersive  $X_3$  phonon mode as a primary order parameter of the Verwey transition which splits the four Fe B sites into two subclasses. This agrees rather well with our observation.

We have undergone the task of simulating various X-ray spectroscopic measurements on the basis of our model. In particular, we focused on comparing  $L_3$  XMCD [2, 7] and  $L_3$  RIXS [7] measurements to our simulations. Our model can reproduce the experimental data and notably it captures the recently reported  $L_3$  RIXS angular dependence well. The existence of this dynamical distortion is furthermore supported by various experimental work such as diffuse scattering experiments using both neutrons [37] and X-rays [38], EXAFS [39], anomalous phonon broadening [40], and pump-probe X-ray diffraction and optical reflectivity [41].

The presence of four non-equivalent Fe B sites in the high temperature phase has rather interesting implications. Overall, we find that the average orbital magnetic moment deduced by XMCD and RIXS-MLAD is the same ( $0.26 \pm 0.03 \mu_B$  per unit formula of  $\text{Fe}_3\text{O}_4$  as illustrated in Fig. 1b and Fig. 4f), however the RIXS-MLAD measurement demonstrates that the average quantity is not sufficient to describe the orbital magnetic moment in  $\text{Fe}_3\text{O}_4$ . This is a result of the non-collinear orbital



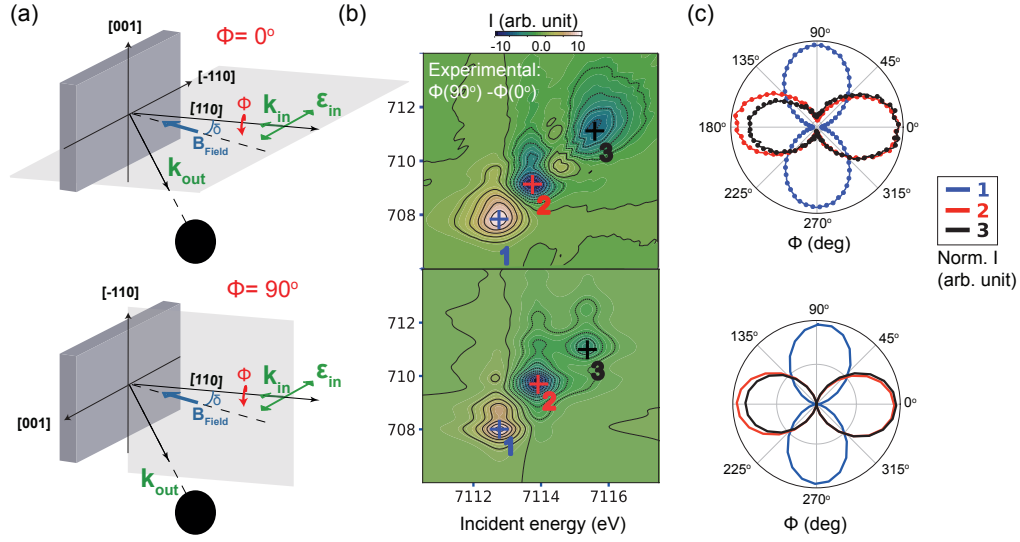


FIG. 2. Fe  $1s2p$  RIXS-MLAD measurements. (a) A sketch of the scattering geometry employed. The magnetic field ( $\mathbf{B}_{Field}$ ) is aligned **nearly** parallel to the incident wave-vector ( $\mathbf{k}_{in}$ ) which corresponds to the [110] direction. (b) Experimental and theoretical dichroism RIXS planes computed as the difference between the RIXS plane at  $\phi = 90^\circ$  and at  $\phi = 0^\circ$ . The full experimental (dotted) and theoretical (solid) 360° RIXS-MLAD signals of the features labelled 1, 2 and 3 in the RIXS dichroism maps are shown in (c) respectively. The angular dependence signal is normalized as:  $RIXS - MLAD = \frac{RIXS(\phi) - Min[RIXS(\phi)]}{Max[RIXS(\phi) - Min[RIXS(\phi)]}$ .

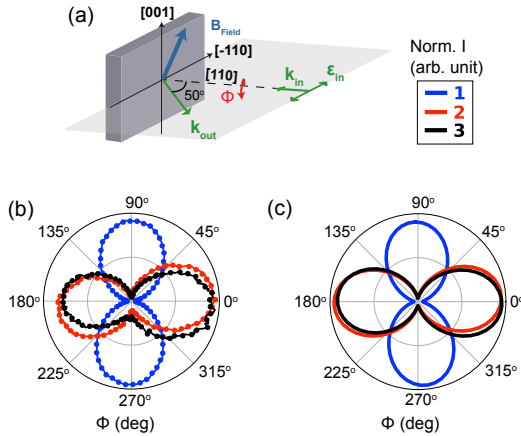


FIG. 3. Fe  $1s2p$  RIXS-MLAD measurements. (a) A sketch of the scattering geometry employed. The magnetic field ( $\mathbf{B}_{Field}$ ) is aligned to the  $[\frac{-\cos(40^\circ)}{\sqrt{2}}, \frac{\cos(40^\circ)}{\sqrt{2}}, \sin(40^\circ)]$  direction. The angular dependence is measured by rotating the sample about the [110] direction ( $\phi$  rotation).  $\phi = 0^\circ$  is defined when the incident polarization vector ( $\boldsymbol{\epsilon}_{in}$ ) is aligned to the [-110] direction. The experimental (dotted) and calculated (solid) angular dependence of the three main features (labeled 1, 2 and 3) are shown in panels (b) and (c).

275 torsion effects (static and dynamical), spin-orbit coupling  
 276 and exchange interaction at the formal  $Fe^{2+}$  ions. The  
 277 **orbital magnetic moment** per  $Fe^{2+}$  ion is predicted to  
 278 have a strong dependence on the magnetic field in con-  
 279 trary to the spin magnetic moment which is collinear to  
 280 the magnetic field. Fig. 4 illustrates the dependence of  
 281 the **orbital magnetic moments** on the orientation of the  
 282 magnetic field when we rotate it about the [110] direc-  
 283 tion for the four sites independently. Large non-collinear  
 284 orbital contributions that tilt as much as  $82^\circ$  away from  
 285 the magnetic spin moment orientation are present. Fur-  
 286 thermore, the collinear contribution per site ranges from  
 287 0 to 150% of the average quantity as a function of the  
 288 orientation of the field. Remarkably, the average **orbital**  
 289 **magnetic moment** for the four sites remains nearly con-  
 290 stant (Fig. 4f).

291 The large discrepancies regarding the **orbital magnetic**  
 292 **moment** of Fe in  $Fe_3O_4$  can now be understood in light of  
 293 the large non-collinear contribution, the site dependency  
 294 and the magnetic field angular dependence. Experiments  
 295 sensitive to the effective **orbital magnetic moment** yield  
 296 different results to those sensitive to the projected av-  
 297 erage quantity, or the average of the squared projected  
 298 quantity. Moreover, variations as a function of the ori-  
 299 entation of the magnetic field are expected for experi-  
 300 ments sensitive to the non-averaged quantity. **This or-**

274 ordering arising from the interplay between trigonal dis-

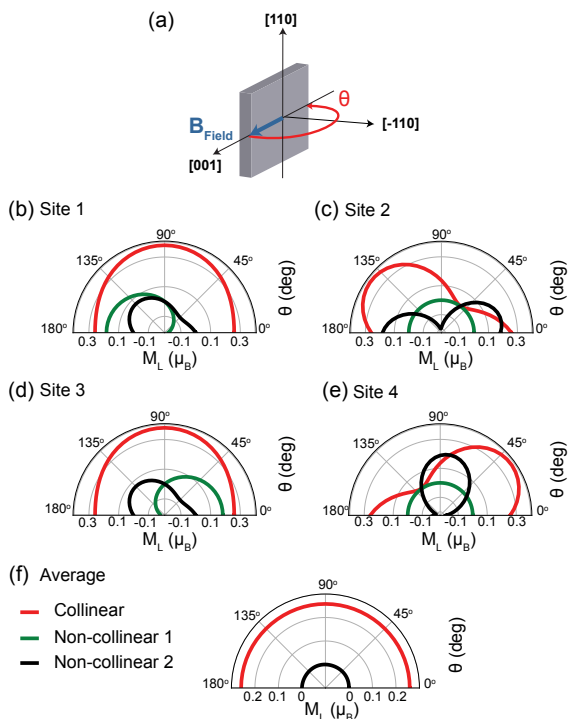


FIG. 4. The angular dependence of the orbital momentum ( $M_L$ ) of the four  $\text{Fe}^{2+}$  ions as a function of the rotation of the magnetic field ( $\mathbf{B}_{\text{Field}}$ ) about the  $[110]$  orientation. (a) Sketch of the rotation geometry. The angular dependence of the orbital momentum projected along the direction of  $\mathbf{B}_{\text{Field}}$  and two perpendicular non-collinear contributions are shown in panel (b), (c), (d) and (e). The average orbital magnetic moments of the four  $\text{Fe}^{2+}$  ions are shown in (f).

dering of the orbital magnetic moment is predicted to be short-ranged due to the dynamical distortions at the high temperature phase of  $\text{Fe}_3\text{O}_4$ . The combination of  $1s2p$  RIXS-MLAD and XMCD provides a powerful tool to quantify site-selectively non-collinear magnetic ordering with bulk sensitivity. Finally, we show that the orbital degree of freedom is an important precursor for the Verwey transition in  $\text{Fe}_3\text{O}_4$  given the fact that it is coupled to a primary order parameter.

We acknowledge the staff of beamlines ID12 and ID26 of the European synchrotron radiation facility for their help in setting up and running the experiments. A. van der Eerden, S. Deelen, P. Theven and H. Vitoux are thanked for their efforts in building up the setup. We are grateful for P. Zimmerman and A. van der Eerden and A. Ismail for assisting during the synchrotron measurements at beamline ID26. We are grateful for the fruitful discussions with G. Subías, J. Garcia, J. Blasco and V. Vercamer. M. Delgado is thanked for provid-

ing and assisting us to use the program CTM4DOC. We thank A. Bosak and M. Hussein for their help with the X-ray diffraction measurements and sample characterisation. Many thanks to R.-P. Wang for the discussions and suggestions. We acknowledge financial support from COST Action MP1306 (EUSpec). M. Sikora acknowledges support from National Science Center of Poland (2014/14/E/ST3/00026). This work was financed by the ERC advanced Grant XRAYonACTIVE No. 340279.

\* [H.M.E.A.Elnaggar@uu.nl](mailto:H.M.E.A.Elnaggar@uu.nl)

† [F.M.D.deGroot@uu.nl](mailto:F.M.D.deGroot@uu.nl)

- [1] E. Goering, M. Lafkioti, S. Gold, and G. Schütz, *J. Magn. Magn. Mater.* **310**, e249 (2007).
- [2] E. Goering, S. Gold, M. Lafkioti, and G. Schütz, *Europhys. Lett.* **73**, 97 (2006).
- [3] D. J. Huang, C. F. Chang, H.-T. Jeng, G. Y. Guo, H.-J. Lin, W. B. Wu, H. C. Ku, A. Fujimori, Y. Takahashi, and C. T. Chen, *Phys. Rev. Lett.* **93**, 077204 (2004).
- [4] E. Goering, *Phys. Status Solidi B* **248**, 2345 (2011).
- [5] E. Arenholz, G. van der Laan, R. V. Chopdekar, and Y. Suzuki, *Phys. Rev. B* **74**, 094407 (2006).
- [6] H. Y. Huang, Z. Y. Chen, R. P. Wang, F. M. De Groot, W. B. Wu, J. Okamoto, A. Chainani, J. S. Zhou, H. T. Jeng, G. Y. Guo, et al., *Nat. Commun.* **8**, 15929 (2017).
- [7] H. Elnaggar, R. P. Wang, S. Lafuerza, E. Paris, A. C. Komerak, H. Guo, Y. Tseng, D. Mcnelly, F. Frati, M. W. Haverkort, et al., arXiv:1811.04836 [cond-mat.str-el] (2018).
- [8] Y. Li, P. A. Montano, B. Barbiellini, P. E. Mijnarends, S. Kaprzyk, and A. Bansil, *J. Phys. Chem. Solids* **68**, 1556 (2007).
- [9] J. A. Duffy, J. W. Taylor, S. B. Dugdale, C. Shenton-Taylor, M. W. Butchers, S. R. Giblin, M. J. Cooper, Y. Sakurai, and M. Itou, *Phys. Rev. B* **81**, 134424 (2010).
- [10] I. Leonov, A. N. Yaresko, V. N. Antonov, M. A. Korotin, and V. I. Anisimov, *Phys. Rev. Lett.* **93**, 146404 (2004).
- [11] M. Coey, *Nature* **430**, 155EP (2004).
- [12] Y. Tokura and N. Nagaosa, *Science* **288**, 462 (2000).
- [13] P. G. Radaelli, *New J. Phys.* **7**, 53 (2005).
- [14] J. Schlappa, C. Schüßler-Langeheine, C. F. Chang, H. Ott, A. Tanaka, Z. Hu, M. W. Haverkort, E. Schierle, E. Weschke, G. Kaindl, et al., *Phys. Rev. Lett.* **100**, 026406 (2008).
- [15] S. B. Wilkins, S. Di Matteo, T. A. W. Beale, Y. Joly, C. Mazzoli, P. D. Hatton, P. Bencok, F. Yakhov, and V. A. M. Brabers, *Phys. Rev. B* **79**, 201102 (2009).
- [16] A. Tanaka, C. F. Chang, M. Buchholz, C. Trabant, E. Schierle, J. Schlappa, D. Schmitz, H. Ott, P. Metcalf, L. H. Tjeng, et al., *Phys. Rev. Lett.* **108**, 227203 (2012).
- [17] A. Tanaka, C. F. Chang, M. Buchholz, C. Trabant, E. Schierle, J. Schlappa, D. Schmitz, H. Ott, P. Metcalf, L. H. Tjeng, et al., *Phys. Rev. B* **88**, 195110 (2013).
- [18] D. Dunlop and O. Özdemir, *Rock magnetism* (Cambridge Univ. Press., 1997).
- [19] E. J. W. Verwey, *Nature* **144**, 327 (1939).
- [20] N. F. Mott, *Rev. Mod. Phys.* **40**, 677 (1968).
- [21] M. Imada, A. Fujimori, and Y. Tokura, *Rev. Mod. Phys.*

- 378 **70**, 1039 (1998).  
379 [22] P. Carra, B. T. Thole, M. Altarelli, and X. Wang, Phys. Rev. Lett. **70**, 694 (1993).  
380  
381 [23] D. I. Khomskii and M. V. Mostovoy, J. Phys. A: Math. Gen. **36**, 9197 (2003).  
382  
383 [24] H. Uzu and A. Tanaka, J. Phys. Soc. Jpn. **77**, 074711 (2008).  
384  
385 [25] M. W. Haverkort, M. Zwierzycki, and O. K. Andersen, Phys. Rev. B **85**, 165113 (2012).  
386  
387 [26] Y. Lu, M. Höppner, O. Gunnarsson, and M. W. Haverkort, Phys. Rev. B **90**, 085102 (2014).  
388  
389 [27] M. W. Haverkort, G. Sangiovanni, P. Hansmann, A. Toschi, Y. Lu, and S. Macke, EPL **108**, 57004 (2014).  
390  
391 [28] T. E. Westre, P. Kennepohl, J. G. DeWitt, B. Hedman, K. O. Hodgson, and E. I. Solomon, J. Am. Chem. Soc. **119**, 6297 (1997).  
392  
393 [29] M. U. Delgado-Jaime, K. Zhang, J. Vura-Weis, and F. M. F. De Groot, J. Synchrotron Radiat. **23**, 1264 (2016).  
394  
395 [30] L. V. Gasparov, D. B. Tanner, D. B. Romero, H. Berger, G. Margaritondo, and L. Forró, Phys. Rev. B **62**, 7939 (2000).  
396  
397 [31] B. Handke, A. Kozłowski, K. Parlinski, J. Przewoznik, T. Slezak, A. I. Chumakov, L. Niesen, Z. Kakol, and J. Korecki, Phys. Rev. B **71**, 144301 (2005).  
398  
399  
400  
401  
402  
403 [32] R. Nemausat, D. Cabaret, C. Gervais, C. Brouder, N. Trcera, A. Bordage, I. Errea, and F. Mauri, Phys. Rev. B **92**, 144310 (2015).  
404  
405 [33] P. Piekarz, K. Parlinski, and A. M. Oles, Phys. Rev. Lett. **97**, 156402 (2006).  
406  
407 [34] P. Piekarz, K. Parlinski, and A. M. Oles, Phys. Rev. B **76**, 165124 (2007).  
408  
409 [35] S. Borroni, G. S. Tucker, F. Pennacchio, J. Rajeswari, U. Stuhr, A. Pisoni, J. Lorenzana, H. M. Rønnow, and F. Carbone, New J. Phys. **19**, 103013 (2017).  
410  
411 [36] J. Cumby and J. P. Attfield, Nat. Commun. **8**, 14235 EP (2017).  
412  
413 [37] Y. Yamada, N. Wakabayashi, and R. M. Nicklow, Phys. Rev. B **21**, 4642 (1980).  
414  
415 [38] A. Bosak, D. Chernyshov, M. Hoesch, P. Piekarz, M. Le Tacon, M. Krisch, A. Kozłowski, A. M. Oleś, and K. Parlinski, Phys. Rev. X **4**, 011040 (2014).  
416  
417 [39] G. Subías, J. García, and J. Blasco, Phys. Rev. B **71**, 155103 (2005).  
418  
419 [40] M. Hoesch, P. Piekarz, A. Bosak, M. Le Tacon, M. Krisch, A. Kozłowski, A. M. Oleś, and K. Parlinski, Phys. Rev. Lett. **110**, 207204 (2013).  
420  
421 [41] S. de Jong, R. Kukreja, C. Trabant, N. Pontius, C. F. Chang, T. Kachel, M. Beye, F. Sorgenfrei, C. H. Back, B. Bräuer, et al., Nat. Mater. **12**, 882EP (2013).  
422  
423  
424  
425  
426  
427